Achieving High Thermoelectric Quality Factor Towards High Figure of Merit in GeTe

Ady Suwardi[a*], Jing Cao[b*], Yunshan Zhao[c,d], Jing Wu[a], Sheau Wei Chien[a], Xian Yi Tan[a,e], Lei Hu[f], Xizu Wang[a], Weide Wang[a], Dengfeng Li[g], Yan Yin[g], Wu-Xing Zhou[h], D V Maheswar Repaka[a], Jingsheng Chen[b], Yun Zheng[i], Qingyu Yan[d], Gang Zhang[j#], Jianwei Xu[a,k#]

[a] Institute of Materials Research and Engineering, 2 Fusionopolis Way, Agency for Science, Technology and Research, Singapore 138634
[b] Department of Materials Science and Engineering, National University of Singapore, Singapore 117575
[c] Department of Electrical and Computer Engineering, National University of Singapore, Singapore 117583
[d] NNU-SULI Thermal Energy Research Center (NSTER) & Center for Quantum Transport and Thermal Energy Science (CQTES) School of Physics and Technology Nanjing Normal University, Nanjing 210023, China.
[e]Department of Materials Science and Engineering, Nanyang Technological University, Singapore 639798
[f] Laboratory for Materials and Structures, Tokyo Institute of Technology, 4259 Nagatsuta, Midori-ku, Yokohama, Kanagawa 226-8503, Japan
[g] School of Science, Chongqing University of Posts and Telecommunications, Chongqing 400065, China
[h] School of Materials Science and Engineering & Hunan Provincial Key Laboratory of Advanced Materials for New Energy Storage and Conversion, Hunan University of Science and Technology, Xiangtan, 411201, China.
[i] Key Laboratory of Optoelectronic Chemical Materials and Devices, Ministry of Education, Jianghan University, Wuhan 430056, Hubei, China
[j] Institute of High Performance Computing, 1 Fusionopolis Way, Connexis, Singapore 138632
[k]Department of Chemistry, National University of Singapore, 3 Science Drive 3, Singapore 117543

[*] Equal contribution: A.S and J.C contributed equally to this work.
[#] Corresponding author: jw-xu@imre.a-star.edu.sg ; zhangg@ihpc.a-star.edu.sg

Keywords: thermoelectrics (TE), quality factor, electronic transports, thermal transports, doping

Abstract

In recent years, GeTe has received tremendous attention from the research community due to its favorable electronic and thermal properties which make it one of the best performing thermoelectric compounds. In many reports, high performance has often been achieved via various doping/alloying methods, which typically involve more than one type of dopants. In contrast to the widely used co-doping strategies, this work only uses a minute amount of 1% doping, giving rise to one of the highest quality factor (1.30) at 673 K amongst GeTe, with a corresponding zT of 1.5. The high performance is attributed to simultaneously improved electronic properties via carrier concentration optimization as well as reduced thermal conductivity via additional phonon scattering brought about by In-mass fluctuations. More importantly, we elucidate on the importance of preserving the high quality factor via choosing the right dopants to optimize the carrier concentration. Furthermore, we showed that the strategy of evaluating the quality factor can be applied to other material systems, serving as a general guideline for thermoelectric materials design. The quality factor of GeTe in this work is superior to most other high-performing chalcogenides such as PbTe, SnTe, and SnS, revealing the large space for further enhancing its zT.

Introduction

Thermoelectric material is unique in the way that it converts heat to electricity and vice versa without any need for phase transition or moving parts. However, in the past few decades, its commercial applications did not go beyond niche areas such as radioisotope thermoelectric generators used by National Aeronautics and Space Administration (NASA).[1] This is mainly due to its inferior performance as compared to its traditional competitors, such as compressor-based coolers, internal combustion engine, or even photovoltaics based materials. The figure of merit, zT, which characterizes the intrinsic performance of a thermoelectrics, can be defined as $zT = S^2\sigma T/(\kappa_L + \kappa_e)$ with S, σ, κ_L and κ_e representing Seebeck coefficient, electrical conductivity, lattice and electronic thermal conductivity, respectively. These properties are highly interdependent, and thus overall optimization of these parameters remains challenging. The intricate interdependencies can be best illustrated by the Mott's formula for Seebeck coefficient and Drude model in the degenerate limit of carrier concentration (*i.e.* $n > 1 \times 10^{20}$ cm^{-3}):

$$S = \frac{8\pi^2\kappa_B^2 T}{3eh^2} m_s^* \left(\frac{\pi}{3n}\right)^{2/3} \quad (1)$$

$$\sigma = ne\mu = \frac{ne^2\tau}{m_c^*} \quad (2)$$

The above equations show that the S and σ are inter-related through n and m^*. Tuning n can only result in optimized values of S and σ, while having a high value of m_s^* (density of states effective mass) as compared to m_c^* (inertial effective mass)can result in simultaneously enhanced S and σ . The ratio between m_S^* and m_c^* ($N_V^{*2/3} = m_s^*/m_c^*$) can be independently tuned to maximize both S and σ. N_V^* (valley degeneracy) quantifies the effective number of electronic bands contributing to transports. Enhancing N_V^* can be achieved via band-convergence strategy which results in increased Seebeck coefficient without sacrificing too much of the electrical

conductivity.[2-4] In addition to band convergence, nanostructuring, nanocomposites, as well as defect-induced phonon scattering are widely used to reduce lattice thermal conductivity, which is also independent of other parameters.[5-15] Furthermore, with the advent of high-throughput computational tools, the new materials discovery driving thermoelectrics based on the established physical criteria such as low effective mass and band convergence has also gained popularity.[16-22]

Among the known thermoelectric compounds to date, GeTe has been touted as a promising compound that can potentially rival its famous lead-based counterpart PbTe, as well as other high performing compounds such as SnSe.[23, 24] The allure of this compound lies in its electronic band structure.[25] Due to multiple bands lying at energy levels close to each other, band-convergence is relatively easy to be achieved in this compound. This is especially true near the rhombohedral to cubic phase transition temperature. Despite this advantage, GeTe has largely been overlooked for a long time because of its tendency to form Ge-vacancies, which resulted in extremely high holes concentration and low *zT*. Not surprisingly, for the past few decades, GeTe has mainly been used as alloy for other matrix, such as $(GeTe)_x$-$(AgSbTe_2)_{1-x}$, or PbTe-GeTe alloys.[26, 27] More recently, most of the works on GeTe as the matrix compound have focused on carrier concentration optimization by counter-doping it with a cation of higher valence (i.e. Bi or Sb).[28-37] Other strategies to reduce the hole concentration including doping or alloying with Ti, Cr, Bi_2Te_3, PbTe, Cu_2Te, $AgBiSe_2$, and excess cation as well as heat treatment have also been explored.[29, 31, 38-48] Besides, resonant states introduced via Indium doping and even entropy engineering have also been reported to improve performance.[49, 50] In addition, the fact that GeTe has a rhombohedral structure up to around 700 K makes it less intuitive from the band-convergence point of view due to the low band multiplicity in a lower symmetry compound (*i.e.* the Σ band with N_V of 12 in cubic phase is split into Σ and η bands, each with N_V of 6 but lying in different energy levels in the

rhombohedral phase). Furthermore, strategies to reduce the rhombohedral to cubic transition temperature as well as minimizing the thermal expansion coefficient mismatch have been widely explored.[51-53] To date, many reports on this material have also focused on distorting the rhombohedral structure to near-cubic to achieve a better band convergence.[25, 28, 54-57] This is a successful strategy that has been reported by Juan Li, et al to achieve a record *zT* of 2.4 for GeTe by co-doping Pb and Bi.[58]

While *zT* is a convenient metric to quantify the performance of many thermoelectric compounds, a more holistic approach is to evaluate the quality factor (*B*). The quality factor of a compound is defined as:

$$B = \left(\frac{k_B}{e}\right)^2 \frac{T}{k_L} \sigma_{E_0} \quad (3)$$

where σ_{E_0} and k_L are transport coefficient (which is the carrier concentration-independent conductivity) and lattice thermal conductivity, respectively (more details on σ_{E_0} can be found in supplementary).

In short, the value of *B* represents the maximum potential *zT* for a compound if the carrier concentration is perfectly optimized. A relatively straightforward way to increase *B* is to reduce the lattice thermal conductivity k_L, which has often been achieved through nanostructuring as well as defect engineering.[59] In addition to reducing lattice thermal conductivity, improving the electronic properties via using the electronic fitness function (EFF) as a screening strategies has been proven to be a versatile approach as well.[60]

In this work, we sought to reduce the excess holes concentration in GeTe by introducing excess Ge cation to reduce the Ge vacancies thus reducing the number of holes while at the same

time largely preserving the intrinsic GeTe structure and transport properties so as to achieve high quality factor *B*. 1% In was also added to introduce point-defect which scatters phonons and lowers the lattice thermal conductivity. We found that addition of 1% excess Ge cation as well as 1% In was sufficient to improve the *zT* of this compound by about 100% from around 0.8 to 1.5. Interestingly, a quality factor of 1.30 was obtained in our optimized sample, which is ascribed to our carrier concentration optimization strategy as well as the low lattice thermal conductivity. In addition, we propose that an important reason for the high *zT* of 2.4 reported by Juan Li *et.al.* lies in simultaneous optimization of both the *B* factor as well as the reduced Fermi potential (optimal doping).[58] Lastly, we compared the quality factor of GeTe with other chalcogenides, showing that GeTe is indeed one of the best thermoelectric compounds to date, with superior potential that has yet been unlocked.

Results and Discussions

Figure 1(a) shows the XRD pattern of the final pellets. Minute peaks belonging to elemental Ge were observed for all samples and marked using dotted squares. All peaks can be indexed to rhombohedral GeTe, which represents rock-salt structure distorted in [111] direction. This is consistent with the tendency of Ge to form vacancies and form Ge agglomerations throughout the sample, as shown in Figure 1(b). As the amount of excess Ge increases, the peaks belonging to elemental Ge gets stronger, which serves as an early indication that the efficacy of excess Ge to replace the Ge vacancies is limited. Continuously increasing the amount of excess Ge will not lead to further reduction in the Ge vacancies and the corresponding number of holes in the system, but will result in more elemental Ge precipitates. This is corroborated by the X-ray Fluorescence (XRF) data in Table 1 which shows more than 0.3% decrease in anion fraction (Te%)

between pristine GeTe and $Ge_{1.00}In_{0.01}Te$. Interestingly, the 0.3% decrease in anion fraction corresponds to a reduction of approximately 1.5 x 10^{20} cm^{-3} in holes concentration, which is consistent with the Hall carrier concentration (Table S2). However, negligible difference in anion fraction (Te%) was observed between $Ge_{1.00}In_{0.01}Te$, $Ge_{1.01}In_{0.01}Te$, $Ge_{1.03}In_{0.01}Te$, and $Ge_{1.05}In_{0.01}Te$. Additionally, negligible change was observed between the lattice parameters of the pristine GeTe as well as the $Ge_{1.05}In_{0.01}Te$ samples, as shown in the Rietveld refinement in Figure S1 and Table S1. Figure 1(c) illustrates the role of adding excess Ge cation to reduce the number of Ge vacancies and thus reducing the holes concentration. Additionally, in the low temperature rhombohedral phase, the p-type (holes) carrier transport is mainly through the ∑ band, as shown in Figure 1(d). However, at temperature above the rhombohedral-cubic transition, the L band becomes the dominant transport channel in this compound.

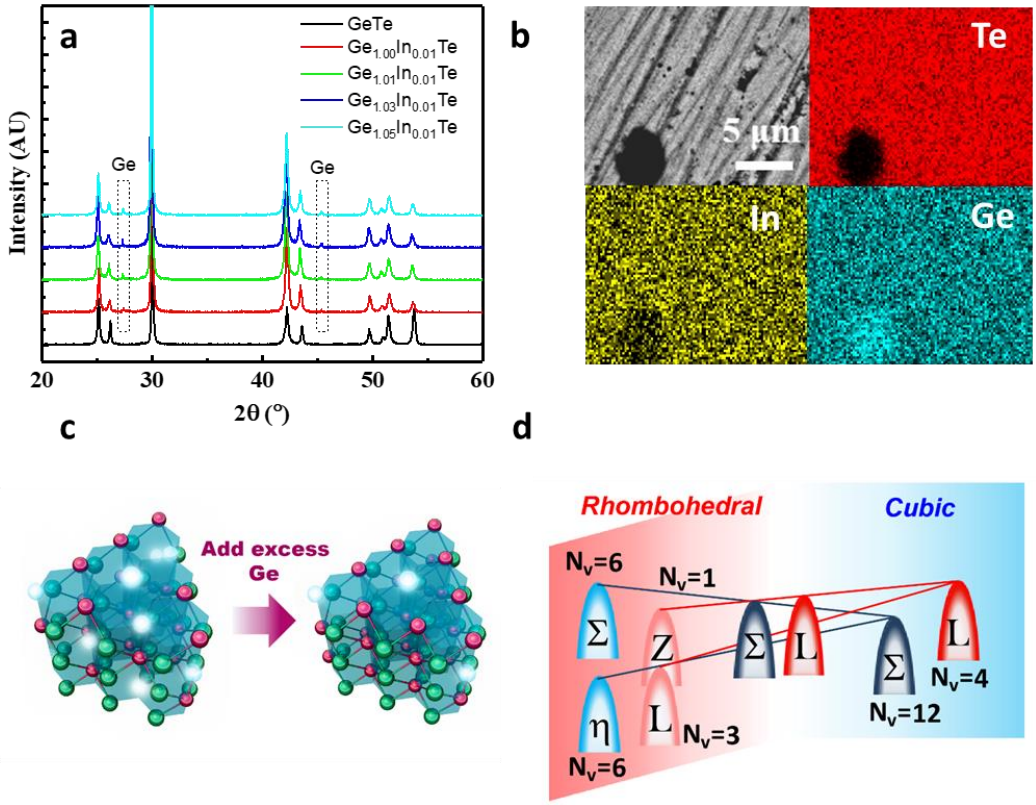

Figure 1. (a) Power XRD patterns of pristine GeTe and In-doped Ge-excess samples. (b) SEM EDS showing uniform distribution of In in GeTe as well as regions with excess Ge. (c) Illustration showing the role of excess Ge in partially suppressing the formation of Ge vacancies. (d) Illustration of band convergence near the phase transition point.

Compound	Ge (at%)	In (at%)	Total Cation(at%)	Anion-Te (at%)
GeTe	46.61	-	46.61	53.39
$Ge_{1.00}In_{0.01}Te$	46.63	0.36	46.99	53.01
$Ge_{1.01}In_{0.01}Te$	46.59	0.37	46.96	53.04
$Ge_{1.03}In_{0.01}Te$	46.65	0.36	47.01	52.99
$Ge_{1.05}In_{0.01}Te$	46.67	0.32	46.99	53.01

Table 1. XRF data showing elemental atomic composition of pristine GeTe and different excess cation with In-doped samples.

The electrical properties of pristine GeTe as well as In-doped GeTe with excess Ge samples are shown in Figure 2. Figure 2(a) shows the Seebeck coefficient of all samples. Compared to pristine GeTe, addition of 1% In and excess Ge cation increases the Seebeck coefficients drastically. This can be attributed to the reduction in holes concentration brought about by In and Ge cation, which also increased the electrical resistivity, as shown in Figure 2(c). Furthermore, the Seebeck coefficient as well as electrical resistivity saturates at $Ge_{1.01}In_{0.01}Te$ and addition of a higher amount of excess Ge does not seem to further increase the Seebeck coefficient nor electrical resistivity, which is consistent with the power factor trend as shown in Figure 2(d).

Figure 2(b) shows the heat flow vs temperature data from differential scanning calorimetry points to the rhombohedral-cubic onset of phase transition at around 600-650 K, which also coincides with band convergence in the cubic phase. Therefore, not surprisingly, the power factor saturates near the phase transition temperature and remains high for the high temperature cubic phase. The electrical resistivity trend which peaks at around the phase transition temperature indicates the carrier redistribution from $\sum$ band dominated rhombohedral phase to L band

dominated cubic phase. This can be ascribed to heavy inter-valley scattering during the carrier redistribution process, which resulted in high electrical resistivity.[9, 34]

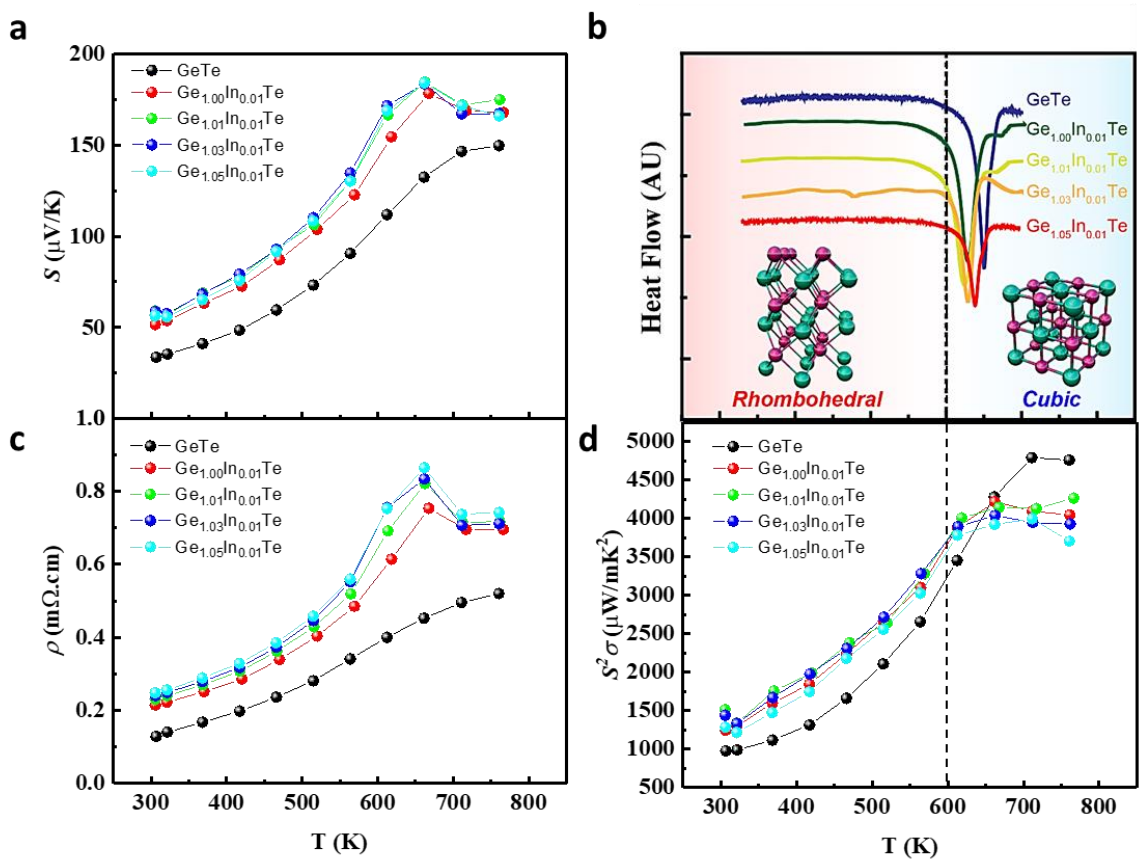

Figure 2. (a) Seebeck coefficient vs temperature (b) Heat flow vs temperature profile of all samples showing structural phase transition from rhombohedral to cubic at high temperature. (c) electrical resistivity vs temperature showing peak around the phase transition temperature. (d) The corresponding power factor which saturates at cubic phase.

Since both Seebeck coefficient and electrical conductivity are function of carrier concentration and are inter-correlated to each other, more insights to the intrinsic electronic transport properties can be derived by analyzing these two parameters together (Jonker analysis), as shown in Figure 3(a). The Seebeck coefficients and the corresponding electrical conductivities for the pristine GeTe and $Ge_{1.01}In_{0.01}Te$ as well as data from other literatures were plotted and compared between each other. The dotted red line represents the relationship between Seebeck and electrical conductivity for transport coefficient values of $\sigma_{E_0} = 1.5 \times 10^5$ S/m while the dotted black

line represents σ_{E_0} = 6.0 × 10^4 S/m. Here, σ_{E_0} represents the carrier concentration-independent electronic transport quality of the compound and is directly related to σ via:

$$\sigma = \sigma_{E_0} \ln(1 + e^{\eta}) \quad (4)$$

where η is the reduced Fermi potential, which is a quantity that has one-to-one correlation to carrier concentration.

It is apparent that the pristine GeTe, $Ge_{1.01}In_{0.01}Te$, as well as other literature reports have similar values of σ_{E_0}, which tells us that all these samples are of similar level of intrinsic electronic transport quality. The value of σ_{E_0} can be associated with the intrinsic charge carrier mobility as well as crystalline quality of the samples. In other words, just by simply performing Jonker analysis on *S vs* σ data, the intrinsic carrier mobility can be compared across samples. This obviates the need for Hall effect measurement which is often inaccurate, especially for low mobility samples.[61] In addition, a quick glance at the *S vs* σ plot enables screening of non-optimal sample, such as the quenched GeTe sample that had not undergone post-quenching annealing, as shown in dotted-black line in Figure 3(a).

Another advantage of analyzing and comparing the σ_{E_0} values lies in the mild temperature dependence behavior of this parameter, as shown in Figure S4, which can be used to gauge the electronic transport quality across a broad range of temperature.[62] Using the values of σ_{E_0}, it is also possible to obtain the weighted mobility μ_W which is made of the product of intrinsic carrier mobility, μ_0 and the density of states effective mass m^*_{DOS} (details on μ_W and σ_{E_0} are shown in supplementary). The temperature dependence values of μ_W vs T is shown in Figure 3(b). Above room temperature, the weighted mobility for all samples decreased as a function of temperature, which is consistent with acoustic phonon scattering transport regime. The vertical dotted line in

the figure 3(b) is added as a guide to the eye to show the onset where the weighted mobility is plateaued, which is intricately linked to increased m^*_{DOS} which compensates the reduction in μ_0. The increase in m^*_{DOS} is originated from the band-alignment between $\sum$ and L band near the structural phase transition temperature, as illustrated in the electronic band structure and its corresponding Fermi surface of $Ge_{1.01}In_{0.01}Te$ at 673 K shown in Figure 3(c) and (d), respectively. Lastly, it is interesting to note that the data by Jingfeng *et.al.* (who used mechanical alloying to synthesize the GeTe phase) showed higher weighted mobility and transport coefficients compared to all other samples and literatures.[40] This can possibly be attributed to the difference in sample preparation method since most reports on GeTe used melting-quenching-annealing in quartz ampoules instead of mechanical alloying.

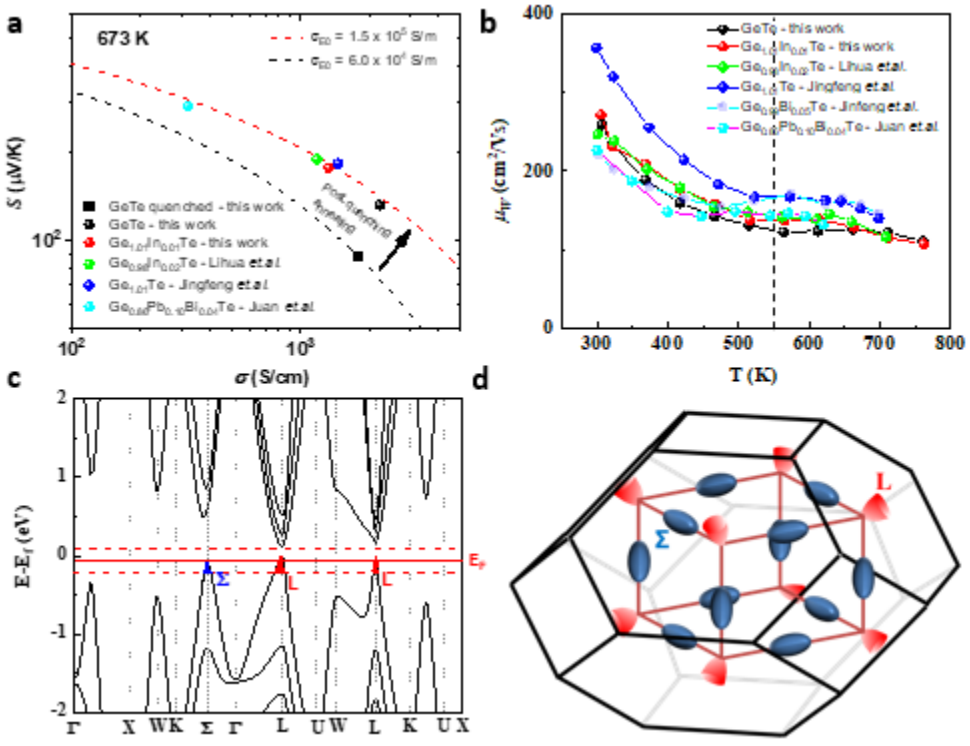

Figure 3. Electronic transport properties of this work in comparison with selected literatures.[40, 49, 58] (a) Seebeck coefficient vs temperature (b) Weighted mobility vs temperature. (c) Electronic band structure of cubic GeTe. The solid red line represents the Fermi level of $Ge_{1.01}In_{1.01}Te$ at 673 K while the dotted red line represents the 3 k_BT range of energies that the majority contribution of the charge carriers are present. (d) The corresponding Fermi surface at the Fermi level shown in (c).

In addition to electronic properties, the reduction in excessive holes concentration as well as mass fluctuations induced by 1% In doping results in lowered thermal conductivity, as shown in Figure 4(a). In order to more accurately estimate the lattice thermal conductivity of our samples, Lorenz number was first calculated using single parabolic band model on the experimental Seebeck and electrical conductivity data of each of our samples (details in supplementary). There are several ways of estimating the Lorenz number with various levels of complexity.[63] The simplest, semi-empirical way of estimating Lorenz number is using: $L = 1.5 + \exp(-|S|/116)$,[64] which was adopted in a few recent GeTe works.[65-67] The method employed in this work is by using the single parabolic band (SPB) model, which is a more accurate version for single parabolic band dominated transport, and also the most widely used. [40, 49, 53, 58] In addition, single Kane band (SKB) model is also widely used, especially in PbTe and SnTe since the valence band maximum for those compounds at low temperature is dominated by L-band, which can be classified as Kane-band.[25, 31, 68] Lastly, it is worth mentioning that the most accurate way of estimating the Lorenz number in materials with band-convergence is using two-band or three-band models which often combines Kane band and Parabolic band modeling.[31, 35, 68]

Due to the fact that all of our Ge excess and In doped samples possess similar values of Seebeck coefficients, their corresponding Lorenz numbers have similar values as well. The temperature dependent Lorenz number for all samples is shown in Figure 4(b). The pristine GeTe sample has higher Lorenz number for all temperatures due to its low electrical resistivity, which results in Lorenz number closer to metallic values (L_0). Figure 4(c) exemplified the benefit of structural phase transition in GeTe: due to carrier re-distribution from the $\sum$ band to the L band, the electrical conductivity dropped to its lowest values near the phase transition temperature. This in turn results in commensurately low electronic thermal conductivity.[65] Further increase in

temperature leads to bipolar conduction, which results in higher electronic thermal conductivity. Lastly, the lattice thermal conductivity of all samples can be estimated by subtracting the electronic thermal conductivity from the total thermal conductivity, as shown in Figure 4(d).

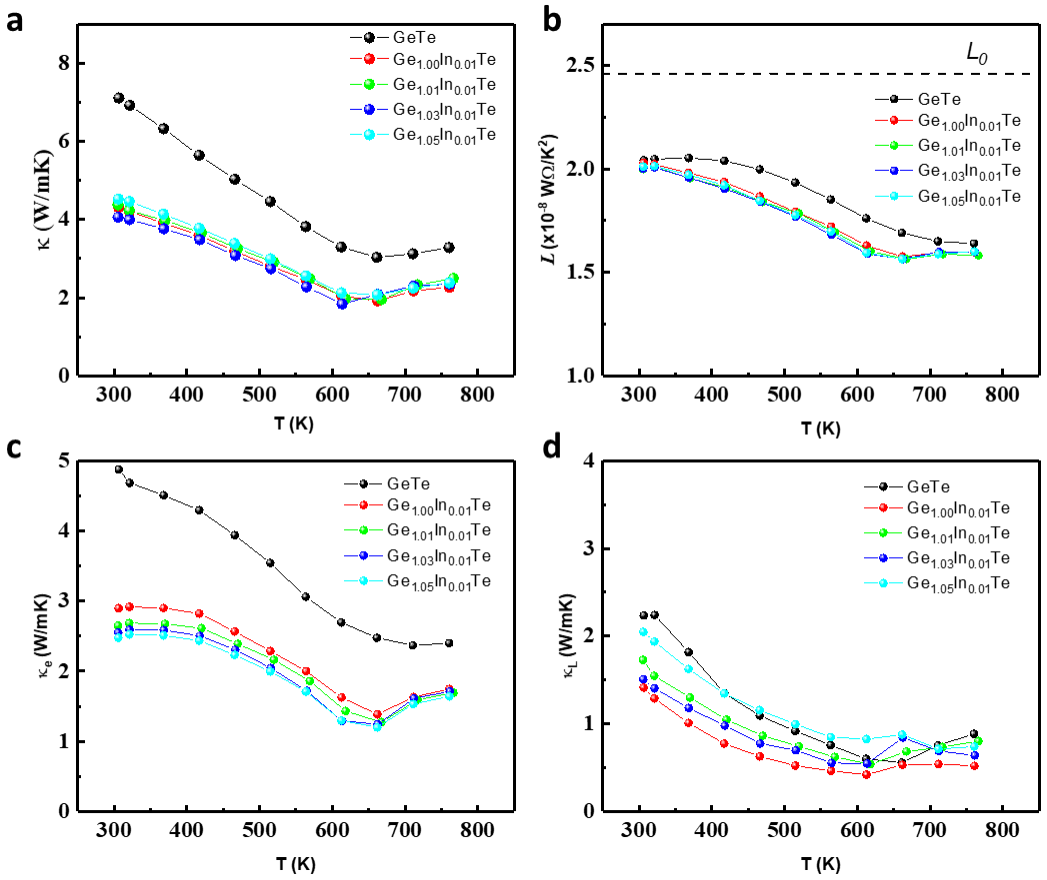

Figure 4. (a) Total thermal conductivity (b) Lorenz numbers as a function of temperature (c) electronic thermal conductivity and (d) lattice thermal conductivity of pristine GeTe and Ge excess + In doped samples.

It is noteworthy that all samples possess very similar values of lattice thermal conductivity with the exception of $Ge_{1.05}In_{0.01}Te$, which can be associated with an excessive amount of elemental Ge which has high frequency vibration modes, therefore high contribution to thermal conductivity. The pristine GeTe showed higher lattice thermal conductivity than GeTe with 1% In doping. This can be explained by the additional phonon scattering induced by the mass-fluctuation from In atoms, which results in lower lattice thermal conductivity. Simplified Debye-Callaway

model was used to further illustrate the role of In induced point defects in reducing the lattice thermal conductivity, as shown in Figure S9, S10, and S11. Interestingly, this stands in contrast to previous report on In-doped GeTe which estimated higher lattice thermal conductivity in In-doped samples.[49] The discrepancy may be associated to different model used to estimate the Lorenz number.[22, 63] Lastly, the lattice thermal conductivities for all samples appear to reach a minimum value of between 0.5 W/mK and 1.0 W/mK in the cubic phase, which leaves further room for reduction to the amorphous limit (0.4 W/mK) of this compound.[7, 58]

Figure 5(a) shows the quality factor, *B* for GeTe in this work as well as literature values for comparison. The details about quality factor and its relationship to weighted mobility and transport coefficients can be found in the supplementary. Each line in Figure 5(a) represents a constant quality factor, with varying zT as a function of reduced Fermi potential, η. It appears to be non-intuitive that the pristine GeTe already possesses a high value of *B* (0.60), but with carrier concentration far from optimal, as indicated by the high value of η, resulting in a low zT. On the contrary, attempts to optimize the carrier concentration by counter-doping of holes using electron-donating elements do not always result in increased *B* factor, as exemplified by the green data point (B = 0.60). It is also interesting to see that in general, counter-doping with Sb seems to have better effect on *B* as compared to counter-doping with Bi, which may be related to the larger size difference brought about by Bi atom, which reduced the intrinsic mobility. Therefore, care must be taken while choosing dopants to optimize the carrier concentration of any material system so as not to sacrifice the *B* factor. The work by Juan Li, *et.al.* serves as a perfect example of optimizing carrier concentration while maintaining a high quality factor. In our optimized sample ($Ge_{1.00}In_{0.01}Te$), we managed to achieve a high quality factor (B = 1.30) while at the same time tuning the carrier concentration towards a more optimal value just by using excess Ge and minute

doping of In, which results in a reasonably high *zT* value of 1.5 at 673 K, as shown in Figure 5(b). In fact, by maintaining *B* =1.30, the *zT* can be further enhanced to 2.5 by further optimizing the carrier concentration. Nevertheless, it is important to note that the B factor is not dependent on reduced Fermi level (or carrier concentration). In fact, the increase in B factor from 0.6 in pristine GeTe to 1.30 in $Ge_{1.01}In_{0.01}Te$ can be attributed to reduction in the lattice thermal conductivity as well as the increase in m^*_{DOS}, which is illustrated by equation (5) and (6).

$$B = \left(\frac{k_B}{e}\right)^2 \frac{T}{k_L} \sigma_{E_0} \tag{5}$$

$$\sigma_{E_0} = \frac{8\pi e (2m_e k_B T)^{3/2}}{3h^3} \frac{e\tau_0}{m_I^*} {m^*_{DOS}}^{3/2} \tag{6}$$

Where k_L, $\sigma_{E_0,}$ and m_I^* represent lattice thermal conductivity, transport coefficient, and inertial effective mass, respectively. It is noteworthy to emphasize that the dramatic enhancements in *zT* near the rhombohedral-cubic phase transition temperature can be attributed to the multifold benefit of electronic band alignment, reduction in electronic thermal conductivity, as well as low lattice thermal conductivity. In short, by analyzing the quality factor (*B*), we are able to determine the efficacy of certain enhancement strategy so as to not only increase the *zT* value, but more importantly to preserve a high intrinsic quality factor for further potential enhancements of the *zT*.

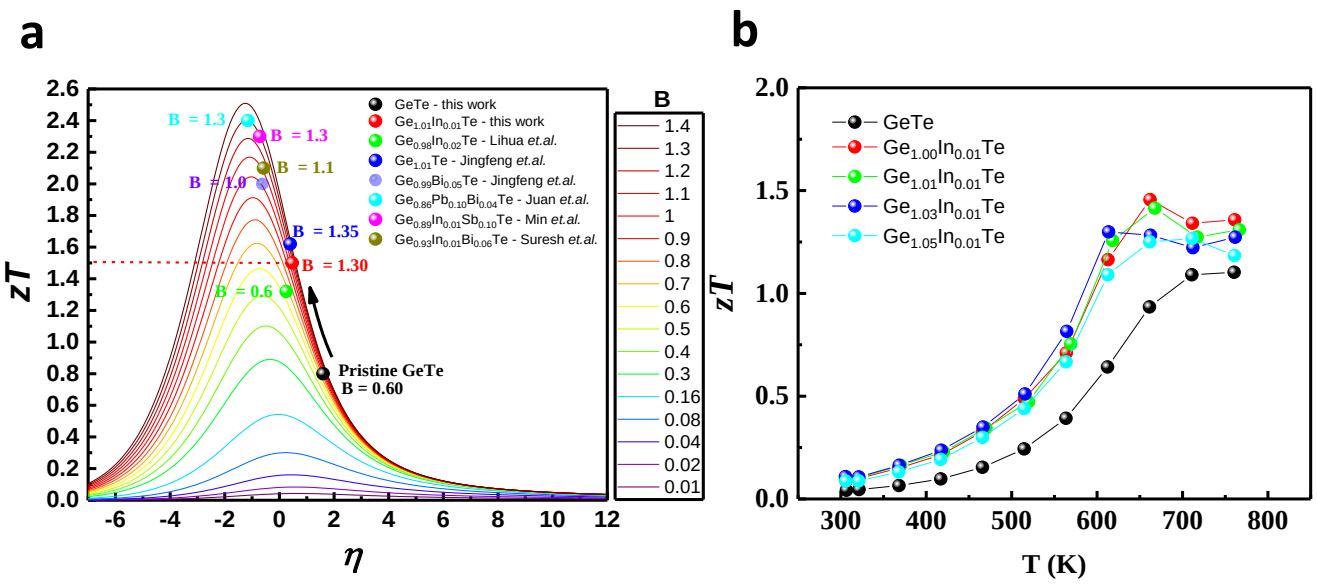

Figure 5. (a) zT as a function of η for different quality factor B for samples in this work as well as literature values for comparison.[32, 33, 40, 49, 58] (b) zT of pristine GeTe as well as In doped and Ge excess samples.

The quality factor evaluation in this work can be applied to other material systems. Figure 6 shows the quality factor of GeTe compared to other high performing chalcogenides, as shown in Figure 6. It can be seen that only SnSe, which possesses B factor of 1.60 in its optimized single crystal form, has a higher quality factor than polycrystalline GeTe. Therefore, somewhat unsurprisingly, the wide attention of the thermoelectric community to this compound in recent years seems justified. Lastly, a common trend that can be observed in Figure 6 is that all of these reports on high-performance binary chalcogenides have the reduced Fermi potential very near the optimal value, which enabled high zT. This observation further reinforces the importance of evaluating the quality factor (B) in addition to zT.

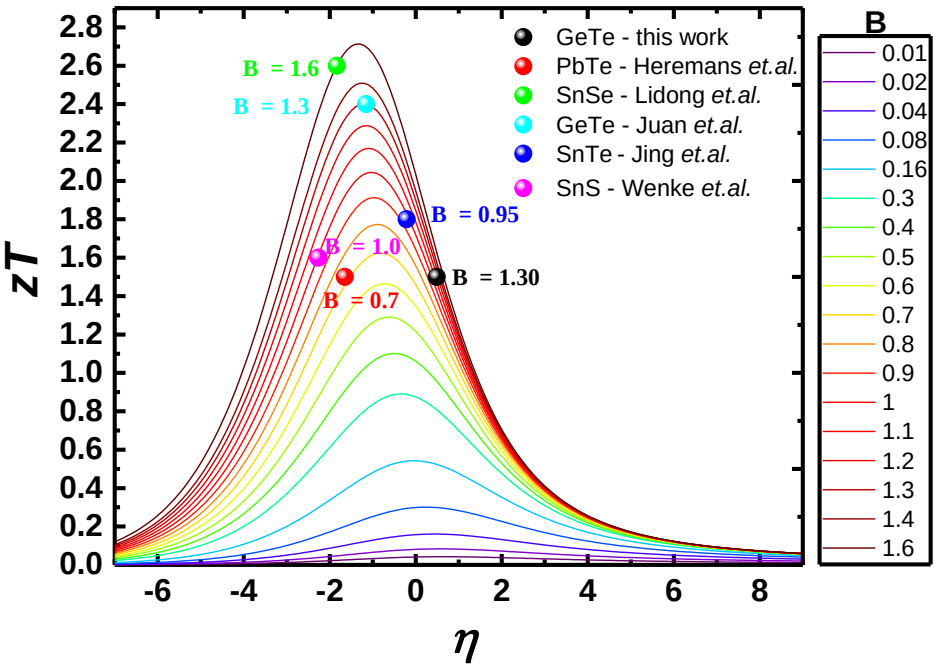

Figure 6. Thermoelectric quality factor of GeTe in this work as compared to other chalcogenides showing highest quality factor for SnSe and GeTe among binary chalcogenide class of materials.[58, 69-72]

Conclusions

In summary, we demonstrated a facile method of optimizing the carrier concentration in GeTe by simply adding excess Ge cation to the compound. We analyzed the intrinsic properties of GeTe in terms of transport coefficient, weighted mobility, as well as quality factor. Indium doping and excess Ge cation was proven to be successful in simultaneously reducing the lattice thermal conductivity as well as optimizing the carrier concentration. In addition, we elucidated on the multifold benefits of rhombohedral-cubic structural phase transition in electronic band alignment, reducing electronic thermal conductivity, as well as minimizing lattice thermal conductivity which results in dramatic *zT* enhancements (*zT* of 1.5) near the phase transition temperature (673 K).

More importantly, we proposed that by utilizing the quality factor (B) analysis, one is able to make a more informed conclusion of whether or not a certain enhancement method is effective. In our work, we achieved a quality factor of $B = 1.30$, which translated to theoretical maximum zT of 2.5 at the most optimal carrier concentration. Furthermore, we showed that in some reports, the dopants used to optimize the carrier concentration in GeTe actually resulted in a lowered quality factor, which translated to limited upside potential for further zT enhancements. Last but not least, we looked into the rationale of the widespread attention to this compound from the intrinsic quality factor point of view, and showed that GeTe has a higher quality factor than most other binary chalcogenides compounds, with the exception of single crystal SnSe.

Experimental Section

Synthesis

Bulk polycrystalline samples of GeTe were prepared by mixing a stoichiometric amount of high-purity element (99.99%) and evacuated to high vacuum of 10^{-5} mbar in quartz ampoules. Samples were subsequently melted at 1223 K for 12 hours, followed by quenching in ice water. Annealing was done at 900 K for 72 hours. The final ingots were then hand ground into fine powder before being consolidated using plasma activated sintering (PAS) at 823 K for 10 minutes under a pressure of 50 MPa. The size of the graphite die was 12.7 mm in diameter. The sintering was done under 1 Pa vacuum. Extra caution was taken during the cooling down by slow cooling at 15 K/min and slowly releasing the pressure to the die to avoid cracking the sample. The final density of the pellets was tested using Archimedes method (~98% theoretical density). Pellets were

then cut and polished into rectangular bars for electrical testing as well as square bars for thermal measurements.

Characterization

Powder XRD patterns were performed on a Bruker D8-Advance X-ray powder diffractometer with Cu Kα radiation. The high temperature Seebeck coefficient and electrical resistivity were measured using ZEM-3 from ULVAC. High temperature thermal conductivity was measured from LFA 457 Netzsch. Experimental heat capacity was used for thermal conductivity determination (Figure S7). It is worth noting that Dulong-Petit value was not used to calculate the thermal conductivity owing to inaccuracies near the phase transition.[73] Microscopy analysis was done in field emission scanning electron microscopy FESEM (JEOL JSM 7600F). The XRF data was collected using M4 Tornado Micro X-ray Fluorescence. The specific heat capacity was measured by Differential Scanning Calorimeter (Mettler Toledo). The sample weight used was around 50 mg that was chip off from pellet, and encapsulated in hermetic pan. Measurement was taken in Nitrogen atmosphere, with heating rate of 2 K/minute.

Band Structures

The lattice parameters and positions of atoms were fully optimized by the projector augmented wave (PAW) method with the Perdew-Burke-Ernzerhof exchange correlation functional implemented in the Vienna ab initio simulation package (VASP).[74] The cutoff energy for the plane-wave basis set was set to 550 eV, and a Monkhorst-Pack k-mesh of 7 × 7 × 7 was used to sample the Brillouin zone, with the energy convergence threshold set as 10^{-6} eV. All atomic positions were relaxed until the maximum atomic force becomes smaller than 0.001 eV/A. The

optimized equilibrium lattice constant of cubic structure GeTe obtained in our calculation was 5.92589 angstrom. For our band structure calculation, we set the lattice parameter to the experimental lattice parameters for pristine GeTe available in supplementary figure S4(d) from Juan.et.al.3 Our optimized equilibrium lattice constant of 5.92589 angstrom is similar to the experimental lattice parameter at 600 K, which is expected to yield more realistic values of band structure. The electronic transport properties were computed within the Boltzmann transport theory in the constant relaxation time approximation, as implemented in the BoltzTrap code.[75] A more dense k-point Monkhorst-Pack mesh with 31×31×31 was adopted for the transport coefficients calculations to guarantee convergence. Once the conductivity and electronic thermal conductivity were obtained, we used the formula to calculate the Lorenz number.

Conflict of Interests

The authors declare no competing financial interest.

Supporting Information

Supporting Information consisting of Reitveld, EDS, SEM, XRF as well as transport analysis, quality factor (B), specific heat capacity, Hall measurements, and Lorenz number caculation.

Acknowledgements

‡ Equal contribution: A.S and J.C contributed equally to this work.

The authors acknowledge support from A*STAR's Science and Engineering Research Council, PHAROS program on Hybrid Thermoelectrics for Ambient Applications: 1527200019, and Agritech program on Sustainable Hybrid Lighting System for Controlled Environment

Agriculture: A19D9a0096. DVM. Repaka acknowledges PHAROS 1527200018. Q. Yan acknowledges Singapore MOE AcRF Tier 2 under Grant Nos. 2018-T2-1-010, Singapore A*STAR Pharos Program SERC 1527200022.

References

1. G. Slack and D. Rowe, *Edition. Rowe DM. Chemical Rubber company. Boca Raton*, 1995, **407**.
2. Y. Pei, X. Shi, A. LaLonde, H. Wang, L. Chen and G. J. Snyder, *Nature*, 2011, **473**, 66-69.
3. L.-D. Zhao, H. Wu, S. Hao, C.-I. Wu, X. Zhou, K. Biswas, J. He, T. P. Hogan, C. Uher and C. Wolverton, *Energy & Environmental Science*, 2013, **6**, 3346-3355.
4. A. Banik, U. S. Shenoy, S. Anand, U. V. Waghmare and K. Biswas, *Chemistry of Materials*, 2015, **27**, 581-587.
5. L. P. Tan, T. Sun, S. Fan, L. Y. Ng, A. Suwardi, Q. Yan and H. H. Hng, *Nano Energy*, 2013, **2**, 4-11.
6. E. S. Toberer, A. Zevalkink and G. J. Snyder, *Journal of Materials Chemistry*, 2011, **21**, 15843-15852.
7. A. Banik, T. Ghosh, R. Arora, M. Dutta, J. Pandey, S. Acharya, A. Soni, U. V. Waghmare and K. Biswas, *Energy & Environmental Science*, 2019, **12**, 589-595.
8. Y. Wu, Z. Chen, P. Nan, F. Xiong, S. Lin, X. Zhang, Y. Chen, L. Chen, B. Ge and Y. Pei, *Joule*, 2019, **3**, 1276-1288.
9. J. Mao, Z. Liu, J. Zhou, H. Zhu, Q. Zhang, G. Chen and Z. Ren, *Advances in Physics*, 2018, **67**, 69-147.
10. Y. Pei, A. D. LaLonde, H. Wang and G. J. Snyder, *Energy & Environmental Science*, 2012, **5**, 7963-7969.
11. G. J. Snyder and E. S. Toberer, in *materials for sustainable energy: a collection of peer-reviewed research and review articles from Nature Publishing Group*, World Scientific, 2011, pp. 101-110.
12. G. Tan, L.-D. Zhao and M. G. Kanatzidis, *Chemical reviews*, 2016, **116**, 12123-12149.
13. A. Zevalkink, D. M. Smiadak, J. L. Blackburn, A. J. Ferguson, M. L. Chabinyc, O. Delaire, J. Wang, K. Kovnir, J. Martin and L. T. Schelhas, *Applied Physics Reviews*, 2018, **5**, 021303.
14. J. Yang, L. Xi, W. Qiu, L. Wu, X. Shi, L. Chen, J. Yang, W. Zhang, C. Uher and D. J. Singh, *npj Computational Materials*, 2016, **2**, 1-17.
15. W. G. Zeier, A. Zevalkink, Z. M. Gibbs, G. Hautier, M. G. Kanatzidis and G. J. Snyder, *Angewandte Chemie International Edition*, 2016, **55**, 6826-6841.
16. A. Suwardi, D. Bash, H. K. Ng, J. R. Gomez, D. M. Repaka, P. Kumar and K. Hippalgaonkar, *Journal of Materials Chemistry A*, 2019, **7**, 23762-23769.
17. J. Recatala-Gomez, A. Suwardi, I. Nandhakumar, A. Abutaha and K. Hippalgaonkar, *ACS Applied Energy Materials*, 2020.
18. E. B. Isaacs and C. Wolverton, *Chemistry of Materials*, 2018, **30**, 1540-1546.
19. J. He, Y. Xia, S. S. Naghavi, V. Ozoliņš and C. Wolverton, *Nature communications*, 2019, **10**, 1-8.
20. J. Yan, P. Gorai, B. Ortiz, S. Miller, S. A. Barnett, T. Mason, V. Stevanović and E. S. Toberer, *Energy & Environmental Science*, 2015, **8**, 983-994.
21. M. Cagnoni, D. Führen and M. Wuttig, *Advanced Materials*, 2018, **30**, 1801787.

22. R. W. McKinney, P. Gorai, V. Stevanović and E. S. Toberer, *Journal of Materials Chemistry A*, 2017, **5**, 17302-17311.
23. Y. Luo, S. Cai, X. Hua, H. Chen, Q. Liang, C. Du, Y. Zheng, J. Shen, J. Xu and C. Wolverton, *Advanced Energy Materials*, 2019, **9**, 1803072.
24. Y. Luo, Y. Zheng, Z. Luo, S. Hao, C. Du, Q. Liang, Z. Li, K. A. Khor, K. Hippalgaonkar and J. Xu, *Advanced Energy Materials*, 2018, **8**, 1702167.
25. J. Li, Z. Chen, X. Zhang, Y. Sun, J. Yang and Y. Pei, *NPG Asia Materials*, 2017, **9**, e353-e353.
26. Z. Z. Luo, X. Zhang, X. Hua, G. Tan, T. P. Bailey, J. Xu, C. Uher, C. Wolverton, V. P. Dravid and Q. Yan, *Advanced Functional Materials*, 2018, **28**, 1801617.
27. Z.-Z. Luo, S. Cai, S. Hao, T. P. Bailey, X. Su, I. Spanopoulos, I. Hadar, G. Tan, Y. Luo and J. Xu, *Journal of the American Chemical Society*, 2019, **141**, 16169-16177.
28. X. Zhang, J. Li, X. Wang, Z. Chen, J. Mao, Y. Chen and Y. Pei, *Journal of the American Chemical Society*, 2018, **140**, 15883-15888.
29. J. Shuai, X. Tan, Q. Guo, J. Xu, A. Gellé, R. Gautier, J.-F. Halet, F. Failamani, J. Jiang and T. Mori, *Materials Today Physics*, 2019, **9**, 100094.
30. L.-D. Zhao, Y. Qiu, Y. Jin, D. Wang, M. Guan, W. He, S. Peng, R. Liu and X. Gao, *Journal of Materials Chemistry A*, 2019, DOI: 10.1039/C9TA10963C.
31. D. Wu, L.-D. Zhao, S. Hao, Q. Jiang, F. Zheng, J. W. Doak, H. Wu, H. Chi, Y. Gelbstein and C. Uher, *Journal of the American Chemical Society*, 2014, **136**, 11412-11419.
32. M. Hong, Z. G. Chen, L. Yang, Y. C. Zou, M. S. Dargusch, H. Wang and J. Zou, *Advanced materials*, 2018, **30**, 1705942.
33. S. Perumal, M. Samanta, T. Ghosh, U. S. Shenoy, A. K. Bohra, S. Bhattacharya, A. Singh, U. V. Waghmare and K. Biswas, *Joule*, 2019, **3**, 2565-2580.
34. M. Hong, J. Zou and Z. G. Chen, *Advanced materials*, 2019, **31**, 1807071.
35. M. Hong, Y. Wang, W. Liu, S. Matsumura, H. Wang, J. Zou and Z. G. Chen, *Advanced Energy Materials*, 2018, **8**, 1801837.
36. S. Perumal, S. Roychowdhury, D. S. Negi, R. Datta and K. Biswas, *Chemistry of Materials*, 2015, **27**, 7171-7178.
37. K. saheb Bayikadi, S. Raman, C. T. Wu, L.-C. Chen, K. H. Chen and F.-C. Chou, *Journal of Materials Chemistry A*, 2020.
38. Y. Jin, Y. Xiao, D. Wang, Z. Huang, Y. Qiu and L.-D. Zhao, *ACS Applied Energy Materials*, 2019, **2**, 7594-7601.
39. K. S. Bayikadi, R. Sankar, C. T. Wu, C. Xia, Y. Chen, L.-C. Chen, K.-H. Chen and F.-C. Chou, *Journal of Materials Chemistry A*, 2019, **7**, 15181-15189.
40. J. Dong, F.-H. Sun, H. Tang, J. Pei, H.-L. Zhuang, H.-H. Hu, B.-P. Zhang, Y. Pan and J.-F. Li, *Energy & Environmental Science*, 2019, **12**, 1396-1403.
41. Y. Gelbstein, J. Davidow, S. N. Girard, D. Y. Chung and M. Kanatzidis, *Advanced Energy Materials*, 2013, **3**, 815-820.
42. M. Samanta and K. Biswas, *Journal of the American Chemical Society*, 2017, **139**, 9382-9391.
43. Z. Bu, W. Li, J. Li, X. Zhang, J. Mao, Y. Chen and Y. Pei, *Materials Today Physics*, 2019, **9**, 100096.
44. M. Samanta, T. Ghosh, R. Arora, U. V. Waghmare and K. Biswas, *Journal of the American Chemical Society*, 2019, **141**, 19505-19512.
45. M. Hong, Y. Wang, T. Feng, Q. Sun, S. Xu, S. Matsumura, S. T. Pantelides, J. Zou and Z.-G. Chen, *Journal of the American Chemical Society*, 2018, **141**, 1742-1748.
46. E. Nshimyimana, S. Hao, X. Su, C. Zhang, W. Liu, Y. Yan, C. Uher, C. Wolverton, M. G. Kanatzidis and X. Tang, *Journal of Materials Chemistry A*, 2020.
47. J. Shuai, Y. Sun, X. Tan and T. Mori, *Small*, **n/a**, 1906921.
48. W. D. Liu, D. Z. Wang, Q. Liu, W. Zhou, Z. Shao and Z. G. Chen, *Advanced Energy Materials*, 2020.

49. L. Wu, X. Li, S. Wang, T. Zhang, J. Yang, W. Zhang, L. Chen and J. Yang, *NPG Asia Materials*, 2017, **9**, e343-e343.
50. Y. Qiu, Y. Jin, D. Wang, M. Guan, W. He, S. Peng, R. Liu, X. Gao and L.-D. Zhao, *Journal of Materials Chemistry A*, 2019, **7**, 26393-26401.
51. T. Xing, Q. Song, P. Qiu, Q. Zhang, X. Xia, J. Liao, R. Liu, H. Huang, J. Yang and S. Bai, *National Science Review*, 2019, **6**, 944-954.
52. Z. Liu, J. Sun, J. Mao, H. Zhu, W. Ren, J. Zhou, Z. Wang, D. J. Singh, J. Sui and C.-W. Chu, *Proceedings of the National Academy of Sciences*, 2018, **115**, 5332-5337.
53. Z. Zheng, X. Su, R. Deng, C. Stoumpos, H. Xie, W. Liu, Y. Yan, S. Hao, C. Uher and C. Wolverton, *Journal of the American Chemical Society*, 2018, **140**, 2673-2686.
54. J. Li, X. Zhang, S. Lin, Z. Chen and Y. Pei, *Chemistry of Materials*, 2017, **29**, 605-611.
55. J. Li, Z. Chen, X. Zhang, H. Yu, Z. Wu, H. Xie, Y. Chen and Y. Pei, *Advanced Science*, 2017, **4**, 1700341.
56. J. Li, X. Zhang, X. Wang, Z. Bu, L. Zheng, B. Zhou, F. Xiong, Y. Chen and Y. Pei, *Journal of the American Chemical Society*, 2018, **140**, 16190-16197.
57. X. Zhang, Z. Bu, S. Lin, Z. Chen, W. Li and Y. Pei, *Joule*, DOI: 10.1016/j.joule.2020.03.004.
58. J. Li, X. Zhang, Z. Chen, S. Lin, W. Li, J. Shen, I. T. Witting, A. Faghaninia, Y. Chen and A. Jain, *Joule*, 2018, **2**, 976-987.
59. H. Wang, Y. Pei, A. D. LaLonde and G. J. Snyder, in *Thermoelectric Nanomaterials*, Springer, 2013, pp. 3-32.
60. G. Xing, J. Sun, Y. Li, X. Fan, W. Zheng and D. J. Singh, *Physical Review Materials*, 2017, **1**, 065405.
61. A. Suwardi, L. Hu, X. Wang, X. Y. Tan, D. V. M. Repaka, L. M. Wong, X. Ni, W. H. Liew, S. H. Lim and Q. Yan, *ACS Applied Materials & Interfaces*, 2020.
62. S. D. Kang and G. J. Snyder, *arXiv preprint arXiv:1710.06896*, 2017.
63. A. Putatunda and D. Singh, *Materials Today Physics*, 2019, **8**, 49-55.
64. H.-S. Kim, Z. M. Gibbs, Y. Tang, H. Wang and G. J. Snyder, *APL materials*, 2015, **3**, 041506.
65. Z. Huang, D. Wang, C. Li, J. Wang, G. Wang and L.-D. Zhao, *Journal of Materials Chemistry A*, 2020.
66. K. S. Bayikadi, C. T. Wu, L.-C. Chen, K.-H. Chen, F.-C. Chou and R. Sankar, *Journal of Materials Chemistry A*, 2020, **8**, 5332-5341.
67. L. Wang, J. Q. Li, C. Zhang, T. Ding, Y. Xie, Y. Li, F. Liu, W. Ao and C. Zhang, *Journal of Materials Chemistry A*, 2020.
68. Y. Pei, X. Shi, A. Lalonde, H. Wang, L. Chen and G. Snyder, *Nature*, 2011, **473**, 66-69.
69. W. He, D. Wang, H. Wu, Y. Xiao, Y. Zhang, D. He, Y. Feng, Y.-J. Hao, J.-F. Dong and R. Chetty, *Science*, 2019, **365**, 1418-1424.
70. J. P. Heremans, V. Jovovic, E. S. Toberer, A. Saramat, K. Kurosaki, A. Charoenphakdee, S. Yamanaka and G. J. Snyder, *Science*, 2008, **321**, 554-557.
71. J. Tang, B. Gao, S. Lin, J. Li, Z. Chen, F. Xiong, W. Li, Y. Chen and Y. Pei, *Advanced Functional Materials*, 2018, **28**, 1803586.
72. L.-D. Zhao, S.-H. Lo, Y. Zhang, H. Sun, G. Tan, C. Uher, C. Wolverton, V. P. Dravid and M. G. Kanatzidis, *Nature*, 2014, **508**, 373-377.
73. M. T. Agne, P. W. Voorhees and G. J. Snyder, *Advanced Materials*, 2019, **31**, 1902980.
74. G. Kresse and J. Hafner, *Phys. Rev. B*, 1996, **54**, 11169.
75. G. K. Madsen and D. J. Singh, *Computer Physics Communications*, 2006, **175**, 67-71.